Nanoscale

Accepted Manuscript

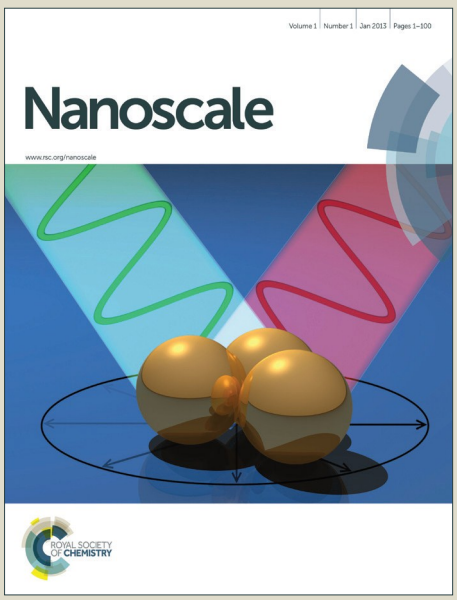

ROYAL SOCIETY OF CHEMISTRY

www.rsc.org/nanoscale

Tuneable Graphene Nanopores for Single Biomolecule Detection

Feras Al-Dirini,[*,1,2,3] *Mahmood A. Mohammed,*[4] *Md Sharafat Hossain,*[1,2,3] *Faruque M. Hossain,*[1,2] *Amapalavanapillai Nirmalathas,*[1,5] *Efstratios Skafidas*[1,2]

[1]Department of Electrical and Electronic Engineering, University of Melbourne, VIC, Australia
[2]Centre for Neural Engineering, University of Melbourne, VIC, Australia,
[3]Victorian Research Laboratory, National ICT Australia, West Melbourne, VIC, Australia
[4]Princess Sumaya University for Technology, Amman, Jordan,
[5]Melbourne Networked Society Institute (MNSI), University of Melbourne, VIC, Australia.
*Email: alf@unimelb.edu.au

Solid-state nanopores are promising candidates for next generation DNA and protein sequencing. However, once fabricated, such devices lack tuneability, which greatly restricts their biosensing capabilities. Here we propose a new class of solid-state graphene-based nanopore devices that exhibit an unique capability of self-tuneability, which is used to control their conductance, tuning it to levels comparable to the changes caused by a translocation of a single biomolecule, and hence, enabling high detection sensitivities. Our presented quantum simulation results suggest that the smallest amino acid, glycine, when present in water and in an aqueous saline solution can be detected with high sensitivity, up to a 90 % change in conductance. Our results also suggest that passivating the device with nitrogen, making it an n-type device, greatly enhances its sensitivity, and makes it highly sensitive to not only the translocation of a single biomolecule, but more interestingly to intramolecular electrostatics within the biomolecule. Sensitive detection of the carboxyl group within the glycine molecule, which carries a charge equivalent to a single electron, is achieved with a conductance change that reaches as high as 99 % when present in an aqueous saline solution. The presented findings suggest that tuneable graphene nanopores, with their capability of probing intramolecular electrostatics, could pave the way towards a new generation of single biomolecule detection devices.

KEYWORDS. Field-Effect, Detection, Graphene, Glycine, Biomolecule, Nanopore, Tuneable.

INTRODUCTION

Nanopore sensors[1, 2] are promising candidates for next generation[3-5] DNA[2, 6] and protein[7-9] sequencing, enabled by their single-molecule detection capabilities.[1, 6, 10-15] Nanopores can be natural,[1, 14] present within protein structures, or artificial,[12] drilled within solid-state materials. Solid-state nanopores[7, 8, 10, 16-26] benefit from robustness and durability,[2] are able to be mass produced[12, 19, 27] and can be integrated with electronic readout and processing circuitry.[28]

When a DNA strand or an amino acid chain in a protein translocate through a nanopore, individual building blocks of their structure, nucleobases or amino acids, can be detected in order to decipher the overall sequence, providing information that can be used in genetic and diagnostic applications.[2, 5, 9, 29] The detection mechanism can be based on measuring the blockage of ionic current travelling through the nanopore, or measuring the modulation of transverse tunneling[30] or conduction[28, 31, 32] current in the device incorporating the nanopore, in response to the translocation of an individual nucleobase or amino acid. The latter method, based on transverse conduction current, has the advantage of easier electronic readout due to higher current levels, but suffers from low sensitivity, due to the relatively small changes in conductance, compared to the originally high conductance of the device, which occur in response to the translocation of single biomolecules.

Solid-state nanopores can be realized using a number of different materials, however, graphene,[31-41] the first two-dimensional material to be isolated,[42] offers a great advantage due to its single atomic thinness,[39] which is comparable to the size of single nucleobases or small amino acids,[39] making it more likely to be affected by their translocation than other types of bulk materials. Once constructed, graphene nanopore biosensors, similar to other types of nanopore biosensors, cannot be controlled or tuned, limiting their ability to robustly distinguish between

different nucleobases or amino acids, let alone be able to detect chemical modifications[24, 43] or structural conformational changes[44] they undergo. Here we propose the realization of a tuneable highly sensitive graphene nanopore biosensor[45] through the incorporation of the nanopore within the channel of another self-tuneable device;[46] the self-switching diode.[47-50]

We study the transport properties and the performance of the proposed tuneable nanopore device using quantum simulations based on Non-Equilibrium Green's Function (NEGF) formalism[51] and the Extended Huckel (EH) method.[52] We investigate how the translocation of the smallest amino acid, glycine, through the nanopore modulates the device's conductivity. Our results show that the device acts as a highly sensitive biosensor being able to selectively detect the translocation of a single glycine molecule in water an in an aqueous saline solution. More interestingly, when the device is passivated with nitrogen, making it an n-type device,[49, 53] our results suggest that the device is able to not only detect the translocation of the glycine molecule, but also detect some of its structural features, namely its carboxyl group, through probing its intramolecular electrostatics.

In the following results and discussion section we describe the structure and operation principle of the proposed tuneable graphene nanopore device and investigate the effect of glycine translocation on its transport properties, when it is passivated with both hydrogen and nitrogen. In the final conclusion section we summarize the findings.

RESULTS AND DISCUSSION

Device Structure

Figure 1 (a) illustrates the geometry of a standard graphene nanopore device, while Fig. 1 (b) illustrates the geometry of a standard self-switching diode. Figure 1 (c) illustrates the proposed tuneable nanopore device, which is a self-switching diode incorporating a nanopore.

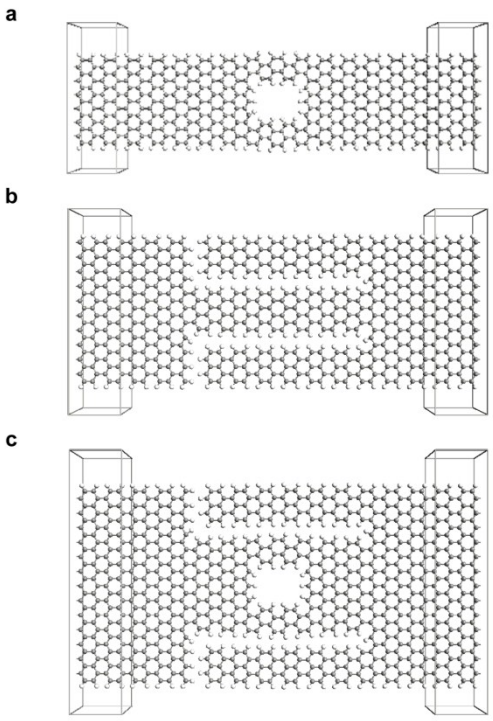

Figure 1 – Comparison between standard and tuneable graphene nanopores. A standard graphene nanopore is shown in (a) and a standard graphene self-switching diode is shown in (b). A tuneable graphene nanopore device, shown in (c), is obtained by incorporating a nanopore, as in (a), within the channel of a graphene self-switching diode similar to the one in (b).

The channel in a self-switching diode is defined by two L-shaped trenches that are etched back-to-back. The conductivity of this channel is controlled by two in-plane side gates that induce an electric field when a bias voltage is applied to the device. This in-plane electric field modulates the distribution of charge carriers within the channel, controlling its conductance. Here we propose incorporating the nanopore, through which translocation occurs, within this channel. The resulting device would have two mechanisms of conductance modulation, one driven by amino acid translocation, which cannot be controlled, and one driven by bias voltage application, which can be controlled. The latter mechanism is used for tuning the device's

original conductance in order to make it comparable to the conductance change caused by the translocation.

The overall structure of the proposed tuneable graphene nanopore device is shown through the schematic illustrations of Fig. 2, presented in top view (Fig. 2 (a)), perspective view (Fig. 2 (b)) and side view (Fig. 2 (c)). The whole device is realized within a single graphene monolayer, by defining a wide nanoribbon and then etching the two L-shaped trenches back-to-back across the width of the nanoribbon. This leaves a narrow nanoribbon channel, defined by the L-shaped trenches, through which conduction occurs. A hole is created within this channel, defining the nanopore, and then all dangling bonds within the device are passivated. Passivation can be achieved by hydrogen or nitrogen,[32, 49, 53] where the latter results in a device with excess free electrons behaving as an n-type device.

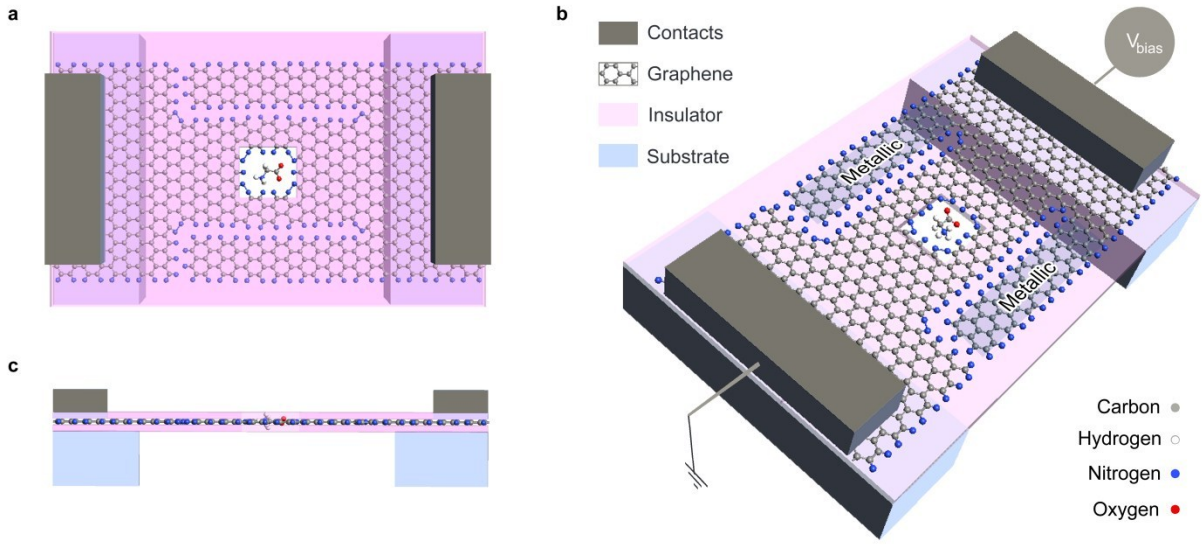

Figure 2 – Schematic illustrations of the geometry of a tuneable graphene nanopore, shown in (a) top view, (b) perspective view and (c) side view. The perspective view illustration (b) shows the applied bias voltage direction and shows how the side gates of the device are chosen to have a width of 3*p*+2 carbon atoms in order for them to behave as if they are metallic and achieve stronger control over the channel's conductivity. In the perspective view illustration the top insulating layer is removed to allow better visualization of the device architecture beneath it.

Finally, after creating the metallic contacts (left and right electrodes) of the device, the device is laminated from the top with an insulating layer to prevent unwanted interaction between it and the biomolecules present in the solution at regions other than the nanopore. This top insulating layer is shown in Figs. 2 (a) and (c), while it is removed from Fig. 2 (b) to allow better visualization of the device architecture beneath it.

The device incorporates two terminals only and does not require a third gate terminal for conductance modulation. Conductance modulation is achieved using the side nanoribbons that are adjacent to the channel of the device, which act as side gates. These side gates are connected to one terminal of the device but are isolated from the other in an asymmetrical geometry that enables the bias voltage to create a potential difference across the channel of the device as well as modulate its conductance at the same time, by means of a self-induced in-plane field effect. The side gates are designed to have widths of $3p+2$ atoms, were p is an integer, in order for them to have vanishingly small bands gaps and behave as if they were metallic, achieving stronger control over the channel's conductivity.[49]

The current-voltage characteristics of the device are similar to self-switching diodes, allowing forward conduction under positive bias voltages that are higher than the threshold voltage of the device, while preventing reverse conduction under reverse bias voltages that are lower than the reverse breakdown voltage of the device. Due to the presence of the nanopore within the channel, these two critical voltages, namely forward threshold voltage and reverse breakdown voltage, occur at lower voltages than in a standard self-switching diode, and hence play critical roles in the operation of tuneable graphene nanopore devices, as will be discussed later on.

Hydrogen Passivation

We begin by studying the hydrogen passivated tuneable graphene nanopore device, shown in Fig. 3 (a), and investigating how the translocation of a single glycine molecule in aqueous solution affects its transport properties. Glycine takes the form of a zwitterion when present in aqueous solution,[54, 55] having a negatively charged carboxyl (COO^-) group on one side and a positively charged amine (NH_3^+) group on the other, creating a dipole within the molecule. However, this dipole does not affect the overall charge of the glycine molecule, which remains to be neutral. We incorporate this glycine molecule into the nanopore of the device of Fig. 3 (a), at two different orientations that are 180° apart, as shown in Figs. 3 (b) and (c).

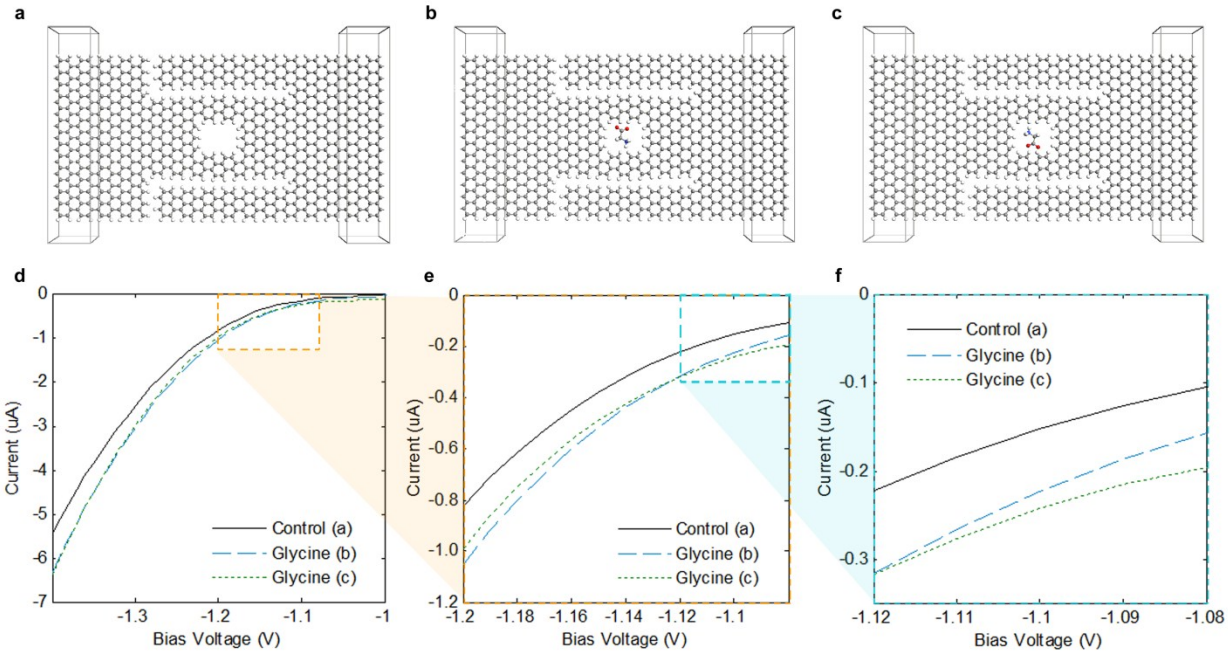

Figure 3 – Glycine detection in aqueous solution using hydrogen passivated tuneable graphene nanopores. Configurations of tuneable graphene nanopores incorporating (a) an empty nanopore, (b) one glycine molecule and (c) the same glycine molecule titled 180°. The I-V characteristics of the devices in (a), (b) and (c) are plotted on the same axes for reverse bias voltages near the reverse breakdown region in (d), zoomed-in near the breakdown point in (e), and zoomed-in furthermore in (f).

The transport properties for the three configurations were calculated using Non-Equilibrium Green's Function (NEGF) Formalism and the Extended Huckel (EH) method as implemented in Atomistix Toolkit (ATK) software package (calculations details are in the Methods section). The current-voltage characteristics of the three configurations are plotted in Fig. 3 (d). A significant difference is observed between the I-V curves of the control case in Fig. 3 (a) (incorporating an empty nanopore) and the two glycine translocations configurations in Figs. 3 (b) and (c) at extreme reverse bias voltages lower than -1 V. This is further highlighted by the zoomed-in regions in Figs. 3 (e) and (f). The figures suggest that the translocation of the glycine molecule results in a significant increase in current levels, occurring consistently for both orientations. Looking at the overall I-V curves for a wider bias range, as shown in Fig. 4 (a), it is observed that this region, in which a large change in conductance takes place, is near the reverse breakdown voltage of the device.

In order to quantify the sensitivity of the device to glycine detection, the absolute change in conductance, relative to the control case, was calculated for the two glycine translocation orientations and averaged in order to get an average absolute change of conductance that resembles these two cases. This is plotted against bias voltage in Fig. 4 (b). It can be clearly seen that the device strongly detects the translocation of the glycine molecule. The device's sensitivity is the highest at the reverse breakdown voltage reaching up to a very high value close to a 90 % change in conductance. This value remains relatively high as the device continues to operate deeper into breakdown under negative voltages lower than -1V. The reason for this, as observed from Fig. 3 (d), is that the presence of glycine within the nanopore results in earlier breakdown. In order to clarify this, a brief illustration of the operation principle of the device under reverse bias is presented through the schematic illustrations of Figs. 5 (a) - (d).

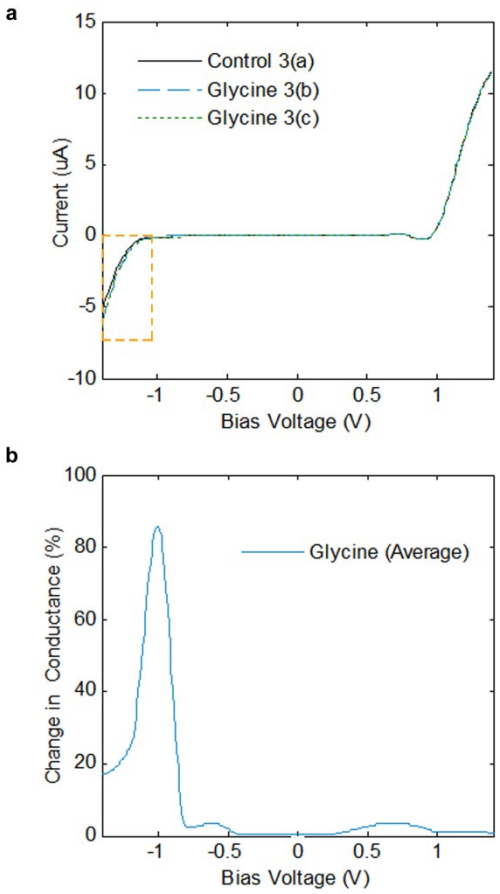

Figure 4 – Glycine detection relative to an empty nanopore. The I-V characteristics of the devices in Figs. 3 (a), (b) and (c), are plotted in (a) across a wide bias voltage range from -1.4 V to 1.4 V. The dotted orange rectangle highlights the portion of the plot in which the device operates in reverse breakdown, which was shown earlier at higher magnification in Fig. 3 (d). The absolute average change in conductance due to the glycine translocation with different orientations (Figs. 3 (b) and (c)) is plotted in (b) against bias voltage.

As Figs. 5 (a) and (b) illustrate, under reverse bias the negative charges that accumulate at the side gates repel electrons within the channel, depleting it from electrons and preventing current flow through the device. As this negative bias is increased, more negative charges are accumulated near the side gates, eventually resulting in the creation of inversion layers at the edges inside the channel, which are regions with excess positive charge carriers; holes. At this point, the channel, which is meant to be off, breaks down and begins to conduct through positive

charge carriers, marking this voltage as the reverse breakdown voltage of the device. The presence of the glycine molecule within the channel seems to shift this reverse breakdown voltage to a lower value, as illustrated through Fig. 3 (d), resulting in higher current values within the reverse breakdown region during glycine translocation. More detailed discussions of the principle of operation of self-switching diodes can be found in earlier work.[46, 49, 50]

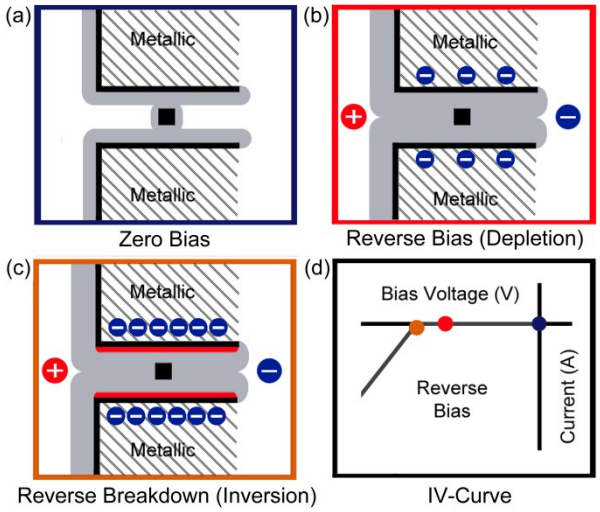

Figure 5 – Schematic illustrations of transport mechanisms within the device under reverse bias. At zero bias (a), marked with a blue circle in (d), the device exhibits natural depletion regions surrounding the insulating trenches as well as the nanopore. As the reverse bias voltage is increased (b), marked with a red circle in (d), the channel eventually becomes completely depleted from electrons due to the accumulation of negative charges near the trenches within the side gates suppressing flow of current through the channel. As the reverse bias voltage is increased further (c), marked with an orange circle in (d), an inversion layer of holes begins to form near the trenches within the channel facilitating charge transport within the channel. This is the reverse breakdown point at which current begins to abruptly increase with any further increase in reverse bias voltage. The expected I-V characteristics of a tuneable graphene nanopore device under reverse bias is plotted in (d), with the positions of zero bias, reverse bias and reverse breakdown mapped on the I-V curve with blue, red and orange circles respectively. The grey regions in (a), (b) and (c) represent regions that are depleted from electrons.

It is important to note that the device experiences the most abrupt change in conductance at the reverse breakdown point, at which an abrupt transition from an off-state to a breakdown state occurs. Therefore, any shift to this breakdown point results in a large change in conductance, as was observed earlier in Fig. 4 (b), hence making the device most sensitive to electrostatic changes within the nanopore when the device is biased near this reverse breakdown voltage.

In the previous investigation glycine translocation was compared to a control case, which was an empty nanopore with no translocation, however, a more meaningful comparison would be between glycine translocation and a control case with water translocation, because glycine would usually be present in solution. We investigate the effect of water translocation through the device by incorporating the maximum number of water molecules that can be present within the device's nanopore at any one time, which is three in this case, as shown in Fig. 6 (a). Another useful comparison would also be with a saline solution, as it is common for proteins and biomolecules to be solvated in saline solutions, and in that case it would be important to investigate if the device is able to selectively detect and distinguish glycine from ionic impurities. In order to investigate this, another configuration is studied, in which the three water molecules translocate through the nanopore along with salth (NaCl), as shown in Fig. 6 (b) (the Na^+ ion is purple in colour and the Cl^- ion is green). The absolute change of conductance of glycine translocation relative to the two new control cases of Figs. 6 (a) and (b), namely water and saline translocations respectively, were calculated and are plotted in Fig. 6 (c). As the figure shows, the sensitivity of the device to glycine translocation relative to water and relative to saline is almost unchanged when compared to Fig. 4 (b) earlier, suggesting that the device is able to selectively detect the translocation of glycine, when present in both water and saline solutions.

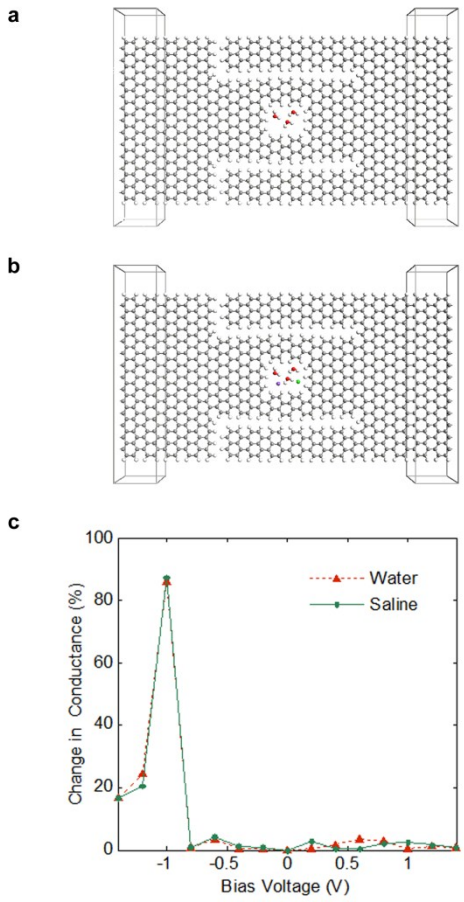

Figure 6 – Glycine detection relative to water and saline. Configurations of tuneable graphene nanopores incorporating (a) three water molecules, (b) three water molecules with salt (NaCl). Absolute average changes in conductance due to the glycine translocation with different orientations (Figs. 3 (b) and (c)) relative to both water translocation (a) and saline translocation (b) are plotted in (c) against bias voltage.

It was noted in Figs. 3 (d) – (f) earlier that the two different glycine orientations (Figs. 3 (b) and (c)) resulted in slightly different current values. This is mainly due to the fact that the glycine molecule is a dipolar molecule with a strong dipole and an asymmetrical structure, and hence the orientation of the molecule within the nanopore and the proximity of the two ends of its dipole (the COO^- and NH_3^+ groups) to the upper and lower sides of the channel surrounding the nanopore greatly affect the conductance of the device, and hence its sensitivity to the detection of glycine translocation. In the two glycine translocation configurations (Figs. 3 (b) and (c)) that

were investigated earlier the two ends of the dipole were in close proximity to the upper and lower sides of the channel surrounding the nanopore, and hence strongly affected the device's overall conductance, as was observed earlier. However, it would be important to investigate a scenario in which the two ends of the dipole are far away from the two sides of the channel surrounding the nanopore, in order to see if the device is still able to detect the translocation of the glycine molecule. Such a configuration can be obtained when the glycine molecule is titled 90^{o} in-plane, as shown in Fig. 7 (a), where the two ends of the dipole are relatively far away from the two sides of the channel surrounding the nanopore. The transport characteristics of this configuration were calculated and compared to the control cases of water and saline translocations.

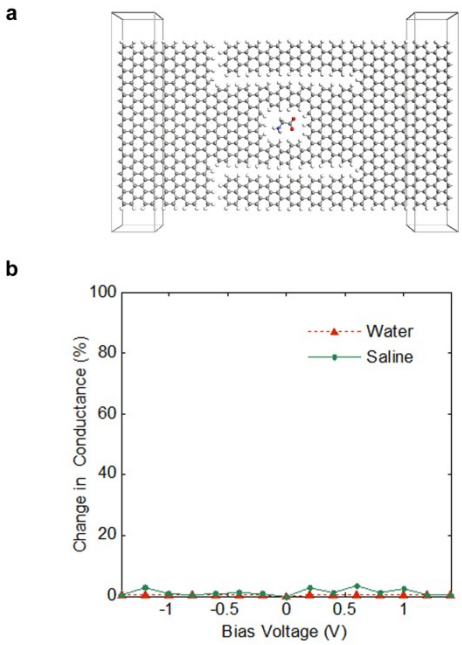

Figure 7 – Glycine (titled 90^{o}) detection relative to water and saline. (a) A configuration of a tuneable graphene nanopore incorporating a glycine molecule tilted 90^{o} in-plane. Absolute change in conductance due to the glycine translocation (a) relative to both water translocation (Fig. 6 (a)) and saline translocation (Fig. 6 (b)) are plotted in (b) against bias voltage.

The absolute change in conductance due to the translocation of the glycine molecule with this orientation (tilted at an angle of 90^{o}) compared to the control cases of water and saline translocations were calculated and are plotted in Fig. 7 (b). The figure suggests that the sensitivity of glycine detection is greatly suppressed when it translocates through the nanopore with such an orientation, indicating a critical limitation in the device's operation as a glycine detector. In order for the device to operate as an efficient glycine detector this limitation needs to be addressed. In order to address this limitation, nitrogen passivation is proposed as a means of enhancing the device's sensitivity, as will be presented in the next section.

Nitrogen Passivation

Passivating a self-switching diode with nitrogen results in an n-type device in which transport is dominated by majority charge carriers, which are negatively charged electrons. It is expected that the presence of excess charge carriers in a tuneable graphene nanopore device would make it more sensitive to electrostatic changes within the nanopore. Moreover, nitrogen passivation lowers the threshold turn-on voltage of the device and makes the change in conductance more abrupt at the transition between the off-state and the on-state at the threshold voltage point, offering another operating point, to add to the reverse breakdown voltage point, in which the device may have increased sensitivity to changes in the electrostatics within the nanopore. Accordingly, we passivated the device of Fig. 1 (c) with nitrogen instead of hydrogen, obtaining the device shown in Fig. 8 (a).

We investigate the effect of glycine translocation through the nitrogen passivated device by placing a glycine molecule within the nanopore of the device. The resulting configuration is shown in Fig. 8 (c). The I-V characteristics of the two devices of Figs. 8 (a) and (c) were calculated and are shown in Fig. 8 (b). The figure shows an enhanced increase in current due to

glycine translocation, when compared to the hydrogen passivated device, under both forward and reverse biases. In both regions the change is most noticeable after the threshold voltage and after the reverse breakdown voltage points. This change is quantified through the absolute change in conductance due to glycine translocation, which is plotted against bias voltage in Fig. 8 (e).

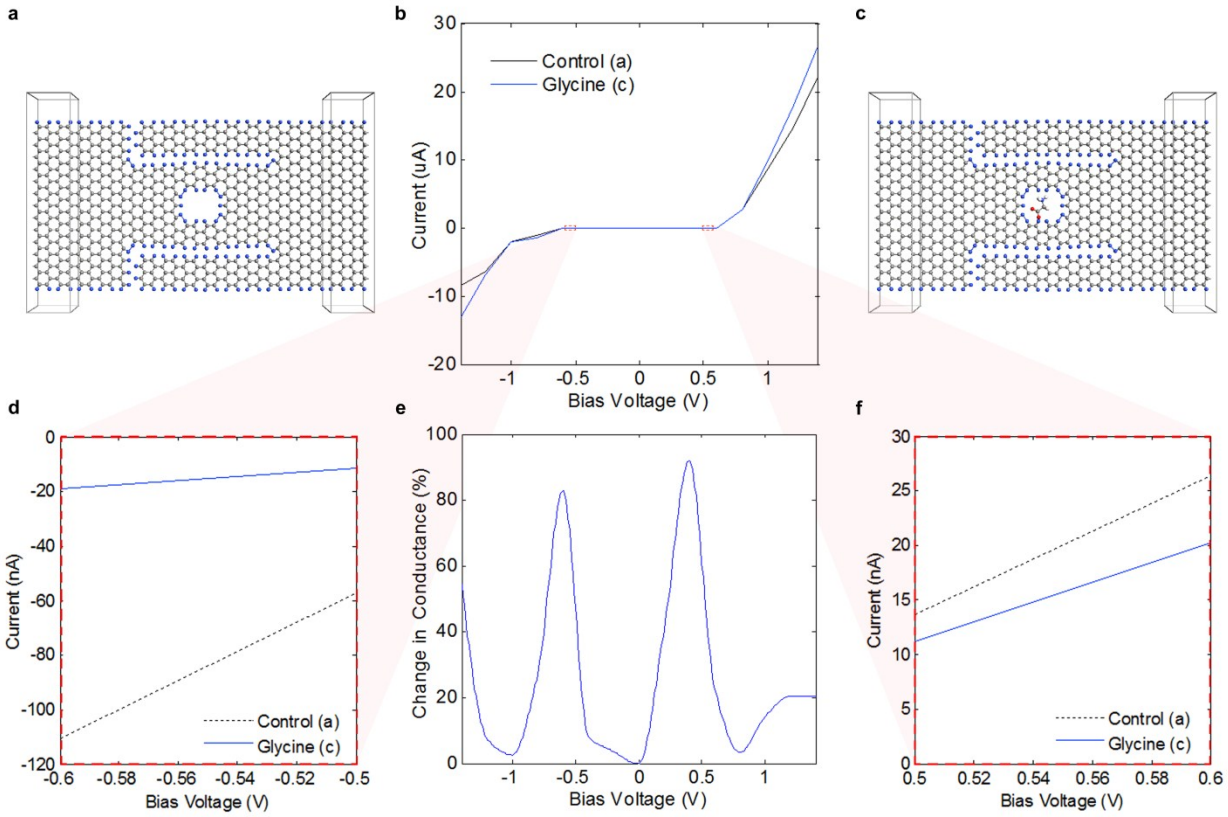

Figure 8 – I-V characteristics of nitrogen passivated tuneable graphene nanorpores with glycine translocation. The structures of nitrogen passivated tuneable graphene nanopore devices with (a) no translocation and (c) glycine translocation, and their I-V characteristics plotted in (b), with a black curve and a blue curve respectively. The resulting absolute change in conductance due to glycine translocation as in (c) relative to no translocation as in (a), is plotted against bias voltage in (e). The plot shows the presence of two unexpected peaks near the reverse breakdown voltage in reverse bias and near the threshold voltage in forward bias. Zoomed-in plots of the I-V curve of (b) are shown in (d) and (f) covering the bias voltage ranges within which the two change-in-conductance peaks appear.

The plot of Fig. 8 (e) suggests relatively high changes at extreme positive and negative voltages reaching close to 50 % under reverse breakdown. However, two very high peaks are observed in the plot near the reverse breakdown and near the threshold voltage points of the device, one being in reverse bias (around – 0.6 V) and the other in forward bias (around 0.6 V). Magnified zoomed-in plots of the I-V characteristics near the bias voltages where the peaks appear are shown in Figs. 8 (d) and (f) for the reverse and forward bias peaks respectively. Both figures suggest that the change in conductance is a decrease in current rather than an increase, suggesting that this change may be driven by a different phenomenon to the changes taking place at higher voltages, and hence requires further investigation.

In order to obtain a deeper insight at the origins of these large changes in conductance, we plot the local transmission pathways within the device under both reverse (- 0.6 V) and forward (0.6 V) biases for the configuration with no translocation (Fig. 8 (a)), in Figs. 9 (a) and (b) respectively, and with glycine translocation (Fig. 8 (c)), in Figs. 9 (c) and (d) respectively. Under reverse bias, with no translocation, the channel of the device is closed with no available transmission pathway, and conduction is dominated by tunneling current through the insulating trenches, as shown in Fig. 9 (a). Tunneling current flows from the left electrode, as well as the channel, into the side gates resulting in the small current values in the nA range seen in Fig. 8 (d). When the glycine molecule translocates through the nanopore (Fig. 9 (c)) tunneling current from the channel to the side gate is suppressed from the lower path in the channel which is adjacent to the carboxyl (COO^-) group of the glycine molecule. This not observed for the upper path of the channel which is adjacent to the amine group (NH_3^+) within the glycine molecule. This can be explained by the fact that the carboxyl group is negatively charged and hence it would repel the negatively charged majority carriers within the channel keeping them away from

the trenches and making it more difficult for them to tunnel across to the lower side gate. However, the amine group is positively charged and would only repel holes, which are minority carriers in an n-type device that do not contribute significantly to the overall conduction.

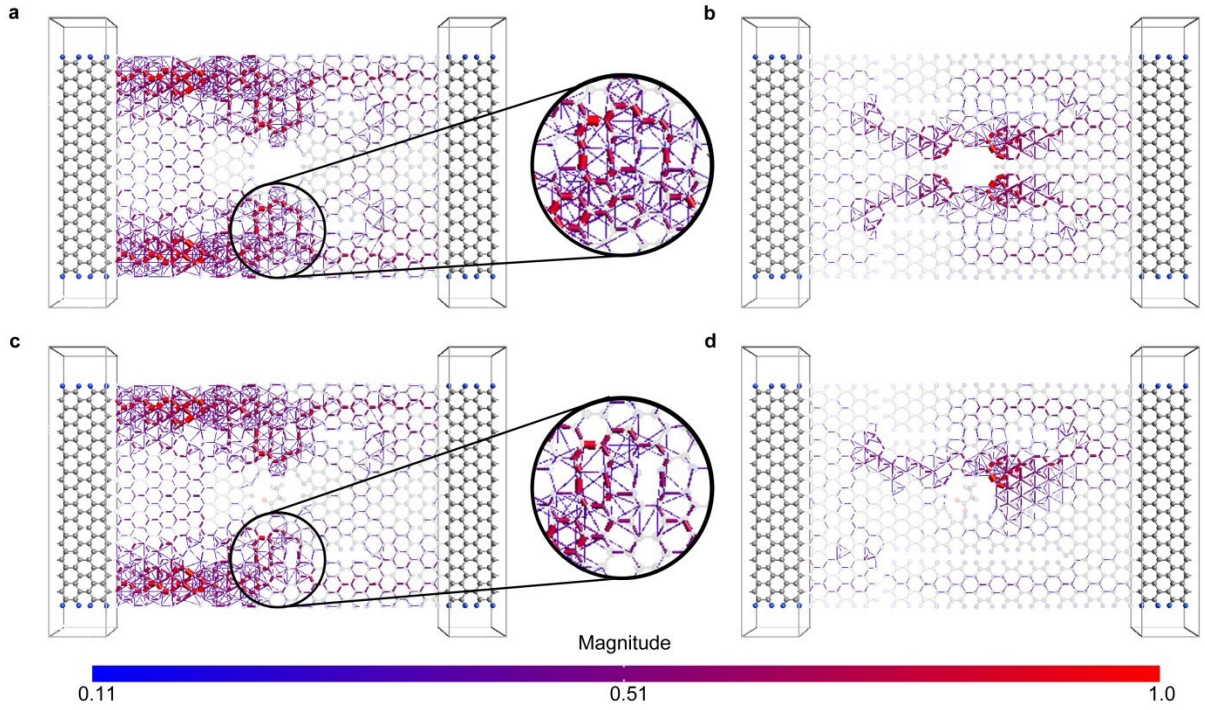

Figure 9 – Detection of the carboxyl group within the glycine molecule. Local transmission pathways for the nitrogen passivated tuneable graphene nanopore device, with no translocation, under (a) a reverse bias of -0.6 V and (b) a forward bias of 0.6 V, and with glycine translocation under (c) a reverse bias of -0.6 V and (d) a forward bias of 0.6 V. Under reverse bias, the zoomed-in portions of (a) and (c) highlight how the proximity of the carboxyl group to the lower side of the channel, during glycine translocation, suppresses tunneling that flows from the channel into the lower side gate. Under forward bias, the transmission pathways within the lower side of the channel are greatly suppressed due to the close proximity of the carboxyl group, which is evident through the comparison of (b) and (d). The magnitudes of the transmission pathways are according to the color bar scale at the bottom of the figure.

Under forward bias, with no translocation (Fig. 9 (b)), the channel begins to open up showing continuous transmission pathways along the length of the channel consistently for both the upper and lower paths. When the glycine molecule translocates through the pore (Fig. 9 (d)), the lower path is completely blocked with no available transmission pathway, reducing the conduction current within the device (Fig. 8 (f)). The upper path is unaffected once again, consolidating the hypothesis that the conductance change is only due to the negatively charged carboxyl group, which repels electrons away from the lower path of the channel depleting it from charge carriers and preventing conduction through it. The absolute change in conductance that results due to the carboxyl group is very high reaching values above 80 % for both the reverse and forward bias cases (Fig. 8 (e)). However, these values are relative to a control case with an empty nanopore, and as with the hydrogen passivated device earlier, it would be more relevant to investigate how the change in conductance due to glycine translocation compares with the control cases of the translocation of water and saline solutions. These two cases are shown in Figs. 10 (a) and (b) for the nitrogen passivated device incorporating three water molecules and three water molecules with salt (NaCl) respectively.

The absolute change in conductance due to glycine translocation (Fig. 8 (c)) relative to the two control cases of water (Fig. 10 (a)) and saline (Fig. 10 (b)) translocations are plotted in Fig. 10 (c). The figure confirms that the device is able to sensitively and selectively detect glycine translocation when present in water and in saline solutions, maintaining its two peaks of large changes in conductance near the threshold voltage and the reverse breakdown voltage of the device, which reach as high as 99 % in saline solutions, confirming the expected enhanced sensitivity of the nitrogen passivated device in comparison to the hydrogen passivated device presented earlier.

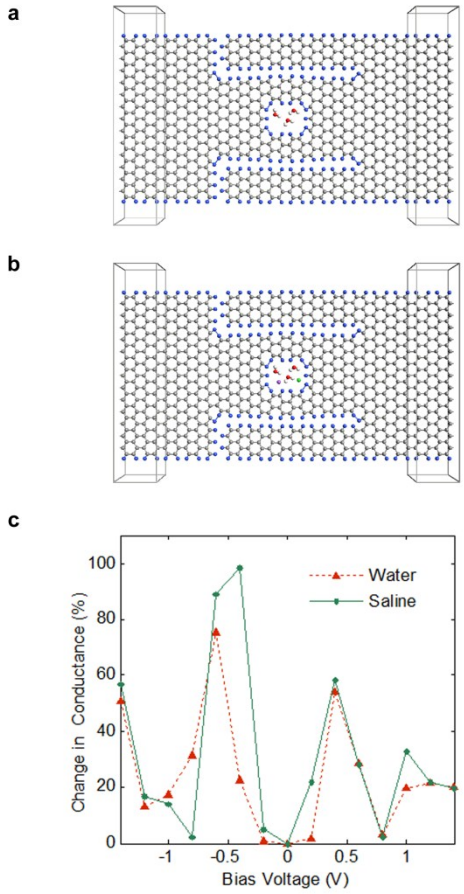

Figure 10 – Glycine detection relative to water and saline for the nitrogen passivated device. Configurations of nitrogen passivated tuneable graphene nanopores incorporating (a) three water molecules, (b) three water molecules with salt (NaCl). Absolute average changes in conductance due to the glycine translocation (Figs. 8 (c)) relative to both water translocation (a) and saline translocation (b) are plotted in (c) against bias voltage.

However, this enhancement would be much more significant if it is able to overcome the limitation of the hydrogen passivated device of not being able to sensitively detect glycine translocation when the glycine molecule translocates with a 90^{o} tilt in its orientation (the point at which the dipole is away from the upper and lower paths of the channel). This glycine translocation orientation is shown in Fig. 11 (a), while Fig. 11 (b) shows the absolute change of conductance due to glycine translocation with this orientation relative to the control cases of water (Fig. 10 (a)) and saline solution (Fig. 10 (b)) translocations plotted against bias voltage.

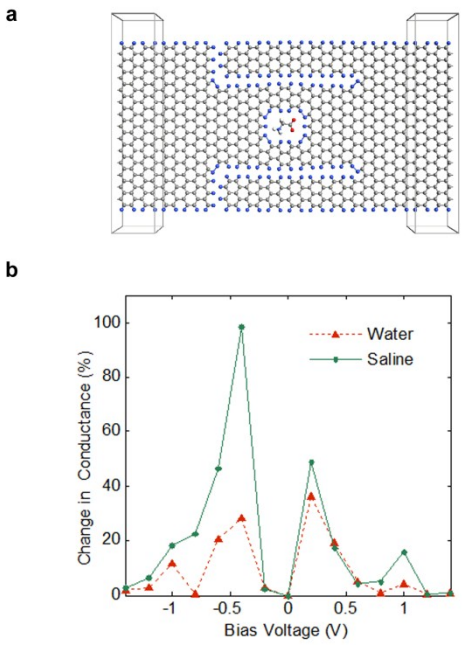

Figure 11 – Glycine (titled 90^{o}) detection relative to water and saline for the nitrogen passivated device. (a) A configuration of a nitrogen passivated tuneable graphene nanopore incorporating a glycine molecule tilted 90^{o} in-plane. Absolute change in conductance due to the glycine translocation (a) relative to both water translocation (Fig. 10 (a)) and saline translocation (Fig. 10 (b)) are plotted in (b) against bias voltage.

It is worth noting here, that in this orientation the negatively charged carboxyl group, to which the device is most sensitive as shown earlier, is at the midpoint between the upper and lower sides of the device's channel, resembling an extreme case scenario. In all other possible in-plane orientations if the carboxyl group is moved away from one side of the channel it will come closer to the other side of the channel. Therefore, it is likely that if this orientation is detectable, then all other possible in-plane orientations would also be detectable. Interestingly, the plot of Fig. 11 (b) suggests that, although the change in conductance is suppressed slightly for a range of bias voltages, as would be expected, the two peaks near the threshold voltage and the reverse breakdown voltage are maintained and continue to reach very high values up to a 99 % change in conductance at reverse breakdown for saline solutions.

These findings suggest that the nitrogen passivated tuneable graphene nanopore device is highly sensitive to intramolecular electrostatics to the extent that it is able to detect an intramolecular structural feature within the glycine molecule carrying charge equivalent to a single electron; a negatively charged carboxyl group, wherever this carboxyl group lies within the nanopore. It is intuitive that larger negative charges would result in larger changes in conductance, while it is postulated that a p-type device dominated by holes, would also be able to selectively detect structural features that carry positive charges, similar to the amine group in glycine.

Finally we would like to clarify that while the process of biomolecule translocation through the nanopore is a dynamic process; all simulations presented in this study were based on a static quantum mechanical (QM) simulation approach. Accordingly, the investigation of different extreme orientations of the glycine molecule translocation was necessary in order to validate the reliability of the detection mechanism. However, further work that can combine the used static QM approach with a dynamic molecular dynamics (MD) simulation approach[56] may prove to be efficient and reliable, as it may take into account other possible orientations of the glycine molecule translocation, including out-of-plane orientations that were not addressed here as well as the possibility of a hydrated configuration with a hydration water shell[57], to add to a range of possible orientations for the translocation of the water molecules and the ionic impurities. Moreover, calculation of noise due to thermo-fluctuations and its comparison to the signal level observed due to glycine translocation through the pore is important future work. This is required in order to study the device's sensitivity and verify its ability to robustly detect glycine in the presence of the expected thermo-fluctuations and would also guide future experimental design.

CONCLUSION

In summary, we have presented a new class of tuneable nanopore biosensors, which can be realized completely within a single graphene monolayer. The device's realization requires minimal process steps and results in a highly sensitive biosensor that is able to detect translocation of single biomolecules. We have demonstrated this through the detection of the smallest amino acid, glycine, in aqueous water and saline solutions. We have also shown how nitrogen passivation makes the device an n-type device with negative majority charge carriers, transforming the device into a highly sensitive electrostatic detector that is capable of detecting intramolecular electrostatic effects as small as a negative charge equivalent to a single electron. We have demonstrated this through the highly sensitive detection of the negatively charged carboxyl group in a glycine zwitterion, which modulates the conductance of the device with a very high change in conductance that reaches as high as 99 % in saline solutions. Our findings suggest a promising potential for the proposed tuneable graphene nanopore biosensor towards the detection of intramolecular electrostatics, which could be an exciting route towards next generation single-biomolecule detection devices.

METHODS

Transport calculations for obtaining I-V characteristic curves and transmission pathway plots were all based on the Extended Huckel (EH) method[52] and Non-Equilibrium Green's Function (NEGF) formalism[51] as implemented in Atomistix Tool Kit (ATK) software package.[58]

Prior to transport calculations, the device geometries were optimized and their coordinates were relaxed using the *Brenner* potential[59] until the forces on individual atoms were minimized to be smaller than 0.05 eV/Å^2.

Calculation of I-V Characteristics

Each device structure was partitioned as three regions: semi-infinite left electrode (L), central scattering region (C), and semi-infinite right electrode (R). The mesh points in real space calculation were defined as uniformly spaced k points of 1 x 10 x 50 for all devices, with 50 sample points along the length (transport direction) and 10 points along the width of the two-terminal structure.

The used tight-binding model was based on the Extended Huckel Method as implemented in ATK-SE package,[58] in which the tight-binding Hamiltonian is parameterized using a two-center approximation, where the matrix elements are described in terms of overlaps between Slater orbitals on each site. The used weighting scheme of the orbital energies of the offsite Hamiltonian was according to Wolfsburg.[60] Further details about the calculation method can be found in Ref. 58.[58]

The electronic transport properties were then calculated using Nonequilibrium Green's Function (NEGF) formalism. The device structure was constructed as the three previously mentioned regions (left-electrode, central-region and right-electrode) and coherent transport of electrons was assumed to occur between left and right electrodes with Fermi levels μ_L and μ_R, respectively, through the central region. According to Landauer's formula,[61] the coherent current between the electrodes is given by:

$$I(V) = \frac{2e}{h}\int_{\mu_R}^{\mu_L} T(E,V)[f_0(E-\mu_L) - f_0(E-\mu_R)]dE \quad (1)$$

where $T(E,V)$ is the transmission probability of incident electrons with energy E from left-electrode (L) to right-electrode (R), $f_0(E-\mu_{L(R)})$ is the Fermi-Dirac distribution function of electrons in the (L) and (R) electrodes respectively, and $V = \frac{\mu_R - \mu_L}{e}$ is the potential difference

between (L) and (R) electrodes. The $T(E,V)$ is correlated with $\hat{G}^a(E)$ and $\hat{G}^r(E)$, the Green's function matrices reflected from L and R to the central scattering region respectively, as:

$$T(E,V) = Tr\left[\mathrm{Im}\sum_L\left(E - \frac{eV}{2}\right)\hat{G}^r(E)\mathrm{Im}\sum_R\left(E + \frac{eV}{2}\right)\hat{G}^a(E)\right] \quad (2)$$

where $\sum_{L(R)}$ are electrodes' self-energies describing the coupling with the central region. The same method was used and is described in previous work.[49, 50, 62-64]

Calculation of Absolute Change in Conductance

The absolute change in conductance, expressed in percentage relative to a controlled case, was calculated in order to quantify the sensitivity of the device to the translocation of different biomolecules, according to the following equation:

$$Absolute\ Change\ in\ Conductance\ (V) = \frac{|I_{trans}(V) - I_{cont}(V)|}{I_{cont}(V)} \times 100 \quad (3)$$

where $I_{trans}(V)$ is the current in the device with the biomolecule positioned within the nanopore, and $I_{cont}(V)$ is the current in the device under one of the three controlled cases: (1) with no translocation, (2) water translocation and (3) translocation of water and salt (saline solution).

Calculation of Transmission Pathways

As the Landauer approach only connects the external electrode current $I(V)$ with the summed energy dependent transmission probability $T(E,V)$, we need to express local current components at the atomic level along the chemical bonds to describe the variation of coherent electron transport through the system. Local current components may be investigated by extracting local transmission components. The total transmission coefficient can be split into local bond contributions, T_{ij}, which are represented in ATK by lines along the bond lengths,

called transmission pathways. The relationship between the total transmission coefficient and the local bond contributions can be described as:

$$T(E,V) = \sum_{i\in A, j\in B} T_{ij}(E,V) \quad (4)$$

where A and B represent pairs of atoms separated by an imaginary surface perpendicular along the bond length. The total transmission coefficient is the sum of the local bond contributions between all pairs of atoms A and B. A negative value of T_{ij} correspond to back scattered electrons along the bond, while a positive value corresponds to transmitted electrons. Further details can be found in Ref. 65.[65]

AUTHOR INFORMATION

Corresponding Author

*Author to whom correspondence should be addressed. Email: alf@unimelb.edu.au.

Author Contributions

F.A.D. conceptualized the tuneable graphene nanopore device concept, and designed and conducted the simulations. All authors analyzed the results and contributed to their understanding. F.A.D. wrote the manuscript and all authors reviewed it.

ACKNOWLEDGMENT

Feras Al-Dirini would like to thank Dana Hirzalla for helping in the production of figures. The authors would like to thank the optics and nanoelectronics research group members for valuable discussions.

REFERENCES

1. Kasianowicz, J. J.; Brandin, E.; Branton, D.; Deamer, D. W. *Proc. Natl. Acad. Sci.* 1996**, 93**, 13770-13773.
2. Venkatesan, B. M.; Bashir, R. *Nat. Nanotechnol.* 2011**, 6**, 615-624.
3. Branton, D.; Deamer, D. W.; Marziali, A.; Bayley, H.; Benner, S. A.; Butler, T.; Di Ventra, M.; Garaj, S.; Hibbs, A.; Huang, X.; Jovanovich, S. B.; Krstic, P. S.; Lindsay, S.; Ling, X. S.; Mastrangelo, C. H.; Meller, A.; Oliver, J. S.; Pershin, Y. V.; Ramsey, J. M.; Riehn, R.; Soni, G. V.; Tabard-Cossa, V.; Wanunu, M.; Wiggin, M.; Schloss, J. A. *Nat. Biotechnol.* 2008**, 26**, 1146-1153.
4. Schadt, E. E.; Turner, S.; Kasarskis, A. *Hum. Mol. Genet.* 2010**, 19**, R227-R240.
5. Voelkerding, K. V.; Dames, S. A.; Durtschi, J. D. *Clin. Chem.* 2009**, 55**, 641-658.
6. Clarke, J.; Wu, H.-C.; Jayasinghe, L.; Patel, A.; Reid, S.; Bayley, H. *Nat. Nanotechnol.* 2009**, 4**, 265-270.
7. Cressiot, B.; Oukhaled, A.; Patriarche, G.; Pastoriza-Gallego, M.; Betton, J.-M.; Auvray, L.; Muthukumar, M.; Bacri, L.; Pelta, J. *ACS Nano* 2012**, 6**, 6236-6243.
8. Firnkes, M.; Pedone, D.; Knezevic, J.; Döblinger, M.; Rant, U. *Nano Lett.* 2010**, 10**, 2162-2167.
9. Oukhaled, A.; Bacri, L.; Pastoriza-Gallego, M.; Betton, J.-M.; Pelta, J. *ACS Chem. Biol.* 2012**, 7**, 1935-1949.
10. Dekker, C. *Nat. Nanotechnol.* 2007**, 2**, 209-215.
11. Hornblower, B.; Coombs, A.; Whitaker, R. D.; Kolomeisky, A.; Picone, S. J.; Meller, A.; Akeson, M. *Nat. Methods* 2007**, 4**, 315-317.
12. Saleh, O. A.; Sohn, L. L. *Nano Lett.* 2002**, 3**, 37-38.
13. Howorka, S.; Siwy, Z. *Chem. Soc. Rev.* 2009**, 38**, 2360-2384.
14. Manrao, E. A.; Derrington, I. M.; Laszlo, A. H.; Langford, K. W.; Hopper, M. K.; Gillgren, N.; Pavlenok, M.; Niederweis, M.; Gundlach, J. H. *Nat. Biotechnol.* 2012**, 30**, 349-353.
15. Mara, A.; Siwy, Z.; Trautmann, C.; Wan, J.; Kamme, F. *Nano Lett.* 2004**, 4**, 497-501.
16. Chang, H.; Kosari, F.; Andreadakis, G.; Alam, M. A.; Vasmatzis, G.; Bashir, R. *Nano Lett.* 2004**, 4**, 1551-1556.
17. Fologea, D.; Uplinger, J.; Thomas, B.; McNabb, D. S.; Li, J. *Nano Lett.* 2005**, 5**, 1734-1737.
18. Iqbal, S. M.; Akin, D.; Bashir, R. *Nat. Nanotechnol.* 2007**, 2**, 243-248.
19. Jijin, Y.; David, C. F.; Lewis, A. S.; Colin, A. S.; Jason, H.; Zheng, R.; Lu-Chang, Q.; Adam, R. H. *Nanotechnology* 2011**, 22**, 285310.
20. Lagerqvist, J.; Zwolak, M.; Di Ventra, M. *Nano Lett.* 2006**, 6**, 779-782.
21. Li, J.; Gershow, M.; Stein, D.; Brandin, E.; Golovchenko, J. A. *Nat. Mater.* 2003**, 2**, 611-615.

22. Li, J.; Stein, D.; McMullan, C.; Branton, D.; Aziz, M. J.; Golovchenko, J. A. *Nature* 2001**, 412**, 166-169.
23. Nicoli, F.; Verschueren, D.; Klein, M.; Dekker, C.; Jonsson, M. P. *Nano Lett.* 2014**, 14**, 6917-6925.
24. Shim, J.; Humphreys, G. I.; Venkatesan, B. M.; Munz, J. M.; Zou, X.; Sathe, C.; Schulten, K.; Kosari, F.; Nardulli, A. M.; Vasmatzis, G.; Bashir, R. *Sci. Rep.* 2013**, 3**, 1389.
25. Storm, A. J.; Storm, C.; Chen, J.; Zandbergen, H.; Joanny, J. F.; Dekker, C. *Nano Lett.* 2005**, 5**, 1193-1197.
26. Wei, R.; Gatterdam, V.; Wieneke, R.; Tampe, R.; Rant, U. *Nat. Nanotechnol.* 2012**, 7**, 257-263.
27. Kim, M. J.; Wanunu, M.; Bell, D. C.; Meller, A. *Adv. Mater.* 2006**, 18**, 3149-3153.
28. Xie, P.; Xiong, Q.; Fang, Y.; Qing, Q.; Lieber, C. M. *Nat. Nanotechnol.* 2012**, 7**, 119-125.
29. Jones, B. *Nat. Rev. Genet.* 2015**, 16**, 68-68.
30. Zwolak, M.; Di Ventra, M. *Nano Lett.* 2005**, 5**, 421-424.
31. Nelson, T.; Zhang, B.; Prezhdo, O. V. *Nano Lett.* 2010**, 10**, 3237-3242.
32. Saha, K. K.; Drndić, M.; Nikolić, B. K. *Nano Lett.* 2012**, 12**, 50-55.
33. Garaj, S.; Hubbard, W.; Reina, A.; Kong, J.; Branton, D.; Golovchenko, J. A. *Nature* 2010**, 467**, 190-193.
34. Merchant, C. A.; Healy, K.; Wanunu, M.; Ray, V.; Peterman, N.; Bartel, J.; Fischbein, M. D.; Venta, K.; Luo, Z.; Johnson, A. T. C.; Drndić, M. *Nano Lett.* 2010**, 10**, 2915-2921.
35. Min, S. K.; Kim, W. Y.; Cho, Y.; Kim, K. S. *Nat. Nanotechnol.* 2011**, 6**, 162-165.
36. Nam, S.; Choi, I.; Fu, C.-c.; Kim, K.; Hong, S.; Choi, Y.; Zettl, A.; Lee, L. P. *Nano Lett.* 2014**, 14**, 5584-5589.
37. Qiu, W.; Nguyen, P.; Skafidas, E. *Phys. Chem. Chem. Phys.* 2014**, 16**, 1451-1459.
38. Sathe, C.; Zou, X.; Leburton, J.-P.; Schulten, K. *ACS Nano* 2011**, 5**, 8842-8851.
39. Schneider, G. F.; Kowalczyk, S. W.; Calado, V. E.; Pandraud, G.; Zandbergen, H. W.; Vandersypen, L. M. K.; Dekker, C. *Nano Lett.* 2010**, 10**, 3163-3167.
40. Wanzhi, Q.; Nguyen, T. C.; Skafidas, E. *IEEE Sens. J.,* 2013**, 13**, 1216-1222.
41. Wells, D. B.; Belkin, M.; Comer, J.; Aksimentiev, A. *Nano Lett.* 2012**, 12**, 4117-4123.
42. Novoselov, K. S.; Geim, A. K.; Morozov, S. V.; Jiang, D.; Zhang, Y.; Dubonos, S. V.; Grigorieva, I. V.; Firsov, A. A. *Science* 2004**, 306**, 666-669.
43. Shim, J.; Kim, Y.; Humphreys, G. I.; Nardulli, A. M.; Kosari, F.; Vasmatzis, G.; Taylor, W. R.; Ahlquist, D. A.; Myong, S.; Bashir, R. *ACS Nano* 2015**, 9**, 290-300.
44. Qiu, W.; Skafidas, E. *ACS Appl. Mater. Interfaces* 2014**, 6**, 16777-16781.
45. Al-Dirini, F.; Hossain, M. S.; Qiu, W.; Hossain, F. M.; Nirmalathas, A.; Skafidas, E. Graphene field effect Nanopore glycine detector, *14th IEEE International Conference on Nanotechnology (IEEE-NANO)*, IEEE, Toronto, Canada, 2014, pp 1004-1007.

46. Song, A.; Missous, M.; Omling, P.; Peaker, A.; Samuelson, L.; Seifert, W. *Appl. Phys. Lett.* 2003**, 83**, 1881-1883.
47. Balocco, C.; Song, A.; Åberg, M.; Forchel, A.; González, T.; Mateos, J.; Maximov, I.; Missous, M.; Rezazadeh, A.; Saijets, J. *Nano Lett.* 2005**, 5**, 1423-1427.
48. Al-Dirini, F.; Skafidas, E.; Nirmalathas, A. Graphene Self Switching Diodes with high rectification ratios, *in 13th IEEE International Conference on Nanotechnology (IEEE-NANO)*, IEEE, Beijing, China, 2013, pp 698-701.
49. Al-Dirini, F.; Hossain, F. M.; Nirmalathas, A.; Skafidas, E. *Sci. Rep.* 2014**, 4**, 3983.
50. Al-Dirini, F.; Hossain, F. M.; Nirmalathas, A.; Skafidas, E. *Nanoscale* 2014**, 6**, 7628-7634.
51. Brandbyge, M.; Mozos, J. L.; Ordejón, P.; Taylor, J.; Stokbro, K. *Phys. Rev. B: Condens. Matter Mater. Phys.* 2002**, 65**, 1654011.
52. Stokbro, K.; Petersen, D. E.; Smidstrup, S.; Blom, A.; Ipsen, M.; Kaasbjerg, K. *Phys. Rev. B: Condens. Matter Mater. Phys.* 2010**, 82**, 075420.
53. Wang, X.; Li, X.; Zhang, L.; Yoon, Y.; Weber, P. K.; Wang, H.; Guo, J.; Dai, H. *Science* 2009**, 324**, 768-771.
54. Hossain, F. M.; Al-Dirini, F.; Skafidas, E. *J. Appl. Phys.* 2014**, 115**, 214303.
55. Hossain, F. M.; Al-Dirini, F.; Skafidas, E. *Appl. Phys. Lett.* 2014**, 105**, 043102.
56. Girdhar, A.; Sathe, C.; Schulten, K.; Leburton, J.-P. *Proc. Natl. Acad. Sci. U.S.A.* 2013**, 110**, 16748-16753.
57. Cohen-Tanugi, D.; Grossman, J. C. *Nano Lett.* 2012**, 12**, 3602-3608.
58. ATK-SE Package. *Quantumwise A/S*. http//www.quantumwise.com (September 27, 2013).
59. Brenner, D. W.; Shenderova, O. A.; Harrison, J. A.; Stuart, S. J.; Ni, B.; Sinnott, S. B. *J. Phys.: Condens. Matter* 2002**, 14**, 783-802.
60. Wolfsberg, M. A. X.; Helmholz, L. *J. Chem. Phys.* 1952**, 20**, 837-843.
61. Landauer, R. *IBM J. Res. Dev.* 1957**, 1**, 223-231.
62. Al-Dirini, F.; Hossain, F. M.; Nirmalathas, A.; Skafidas, E. *IEEE J. Electron Devices Soc.* 2014**, 2**, 118-122.
63. Al-Dirini, F.; Hossain, F. M.; Mohammed, M. A.; Nirmalathas, A.; Skafidas, E. *Sci. Rep.* 2015**, 5**, 14815.
64. Al-Dirini, F.; Mohammed, M. A.; Hossain, F. M.; Nirmalathas, A.; Skafidas, E. *IEEE J. Electron Devices Soc.* 2016**, 4**, 30-39.
65. Solomon, G. C.; Herrmann, C.; Hansen, T.; Mujica, V.; Ratner, M. A. *Nat. Chem.* 2010**, 2**, 223-228.

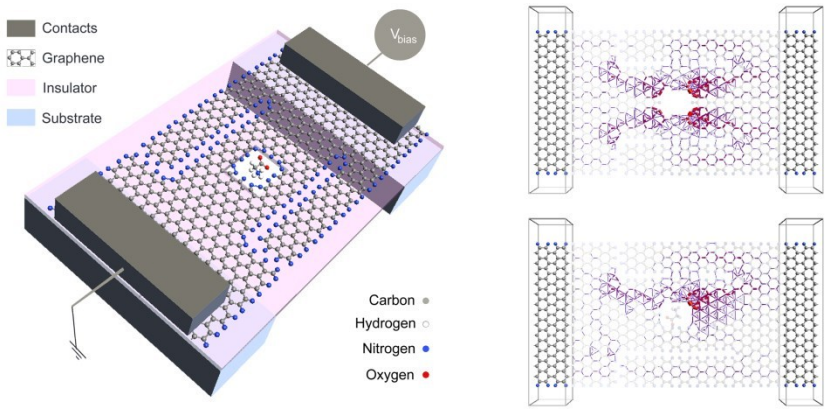

Table of Contents (TOC) Entry:

The architecture of a tuneable graphene nanopore device (left) and the highly sensitive detection of the carboxyl group in a glycine zwitterion as it translocates through the pore (right).